

NASA TM-80138



NASA Technical Memorandum 80138

NASA-TM-80138 19790023076

**THE GEOMETRY OF STELLAR OCCULTATION
MEASUREMENTS ON LONG-DURATION
ATMOSPHERIC MONITORING MISSIONS**

DAVID R. BROOKS

FOR REFERENCE

JULY 1979

NOT TO BE TAKEN FROM THIS ROOM

LIBRARY COPY

AUG 20 1979

**LANGLEY RESEARCH CENTER
LIBRARY, NASA
HAMPTON, VIRGINIA**



National Aeronautics and
Space Administration

Langley Research Center
Hampton, Virginia 23665



THE GEOMETRY OF STELLAR OCCULTATION MEASUREMENTS ON LONG-DURATION ATMOSPHERIC MONITORING MISSIONS

David R. Brooks

Geometrical considerations are presented for analyzing use of the stellar occultation technique on long-duration Earth atmosphere monitoring missions. Simulated mission data are presented for three representative orbits. Bright near-IR stars are used as examples of how extensive global longitude-latitude coverage can be obtained by performing occultation measurements on several stars during the course of a 1-year mission. A brief comparison is made with similar missions using the Sun as a light source.

INTRODUCTION

It has long been recognized that monitoring of light sources from a spacecraft as the sources rise or set on the Earth's horizon is one way to determine the concentration of various atmospheric constituents. Use of the Sun as a source comes immediately to mind and a solar occultation experiment based on orbit analysis done at Langley Research Center¹ is now operational on the SAGE mission.²

Stellar occultation has been successfully used in the past^{3,4,5}, but not as the basic measuring technique for a dedicated atmospheric monitoring mission. The weakness of starlight compared to sunlight is not a major concern, leading only to restrictions on the Sun's position relative to the star during the measurement. As a specific example of such measurements, bright hot stars having maximum emissions in the UV between about 0.15 and 0.30 μ have been used for detecting ozone and molecular oxygen in the mesosphere and thermosphere, respectively.

In this paper, the viewing geometry is considered for long-term stellar occultation measurements from representative Earth orbits. This geometry changes as a function of time as the orbits precess in inertial space. Of particular interest are the distributions of ground coordinates over which the star rises and sets take place, and the associated pointing angles to the Sun.

It is natural to compare the distribution of stellar and solar occultation opportunities for similar orbits; they share most of their features, with the stellar occultation distributions lacking only the seasonal variation imposed by the Sun's apparent motion on the celestial sphere. Clearly, the ground conditions during a solar occultation measurement are limited to dawn or dusk as the Sun is viewed across its terminator on the Earth's surface. Stellar occultations are not limited in this way, providing a

potential advantage. Roughly speaking, successful use of starlight requires that the ground under the measurement (as represented by the tangent longitude and latitude coordinates) be in darkness. This restriction eliminates about half of the geometrically feasible measurements.

STELLAR OCCULTATION GEOMETRY

Fig. 1 illustrates the geometry of stellar occultation. First of all, stars are essentially infinitely far away so that all vectors to a particular star are parallel in the vicinity of the Earth. The starlight can be thought of as producing a terminator on the Earth's surface, and it is this great circle that the spacecraft must view to observe a star rise or set. These events are visible only from the "dark" side of the stellar terminator, along the locus of points a central angle A from the terminator. The angle A is measured a distance $A = \cos^{-1}[r_{\oplus}/(r_{\oplus}+h)]$ along a great circle perpendicular to the terminator, where r_{\oplus} is the radius of the Earth (6378 km) and h is the spacecraft altitude in km.

Given a particular orbit and stellar position, it is possible to predict the range of ground coordinates above which stellar occultations may be observed, and to determine from where in a spacecraft's orbit such measurements can be made. Fig. 2 illustrates the geometry and gives the trigonometric relationships for $0^{\circ} < \ell < 90^{\circ}$ and $0^{\circ} < \delta_s < 90^{\circ}$. These may be used to construct the locus of tangent points and spacecraft coordinates for one quadrant--similar equations pertain to the other quadrants. Fig. 3 shows the spacecraft right ascension and declination coordinates (RA_{SC} and δ_{SC}) from which occultations may be made from a 600-km orbit, for a range of stellar declinations. Declination can be equated to latitude, while right ascension must be related to longitude through an equation which accounts for the Earth's rotation. The zero RA reference is one of the equatorial crossings of the stellar terminator ($RA_{eq} = RA_s + 90^{\circ}$) as shown in Fig. 2. (This reference could be thought of, in a conventional sense, as the "right ascension of the ascending node" of the stellar terminator.) Fig. 4 shows the tangent coordinates (RA_T and λ_T) at which stellar occultations may be viewed as a function of stellar declination. This figure just traces the RA- δ coordinates of the stellar terminator. For a given stellar declination, occultation opportunities occur when a spacecraft groundtrack intersects the locus of points from which the terminator may be viewed; each such opportunity has associated with it a particular measurement coordinate (the tangent point), which will be expressed in a longitude-latitude system.

MISSION ANALYSIS FOR STELLAR OCCULTATION MEASUREMENTS

Three representative Earth orbits have been considered as candidates for stellar occultation missions: a low-inclination, low-altitude orbit such as might be achieved with projected shuttle capabilities (250-km altitude, 28° inclination); a higher-inclination, higher-altitude orbit similar to the SAGE orbit (600-km, 57° inclination); and a Sun-synchronous orbit such as might be used for photographically oriented missions (888-km altitude, 98.988° inclination to give a 1-day repeat cycle). Any of these orbits might involve missions with atmospheric monitoring objectives, having the pointing and stability capabilities required for occultation measurements. A summary of orbit parameters is given in table 1. Each orbit has a particular terminator-viewing capability, set by its inclination and altitude. The latitude range of viewable tangent points (as previously defined) is a parameter of interest. It is easily shown that this range is $\pm|i + A|$, where A is the central angle previously defined. The value of A for each orbit is given in the table. If $\pm|i + A| \geq 90^\circ$, then the entire Earth's surface is available for occultation measurements. Of the three orbits considered, only the Sun-synchronous one has this capability; the latitude range for each orbit is given in the last column of table 1.

A catalog of 158 bright stars is used as the basis for target selection in this paper; table 2* lists their right ascension RA, declination δ_s , visual magnitude m_v , and color temperature T .

Based on the assumption that brighter stars make more desirable targets, all other things being equal, an ordering of the stars is needed. A comparison of visual magnitude or temperature is not sufficient, as the "brightness" of one star relative to another depends on the number of photons incident on sensors limited to a particular band of wavelengths. For this paper, the suitability of stars is based on their output at 1.0μ . In table 3, 10 stars with high output at 1.0μ are listed, along with their output at 0.1μ , 0.55μ , and 10μ . The calculations are done from standard formulae⁶. Using the definition of visual magnitude,

$$m_v = -2.5 \log_{10}(I/I_0)$$

where

$$I_0 = 3.1 \times 10^{-12} \text{ watts/cm}^2$$

*Adapted from Vernam, Peter C.: Star Availability, MIT Aeronomy Program, Charles Stark Draper Laboratory, Internal Report No. AER 10-1, July 7, 1971.

The intensity of the star at 0.55μ , where m_V is defined, is

$$I = I_0 10^{(-m_V/2.5)} \text{ watts/cm}^2$$

The star's blackbody curve, normalized to 1 at its wavelength of maximum power output

$$\lambda_{\max} = 2898/T \mu$$

is given by

$$w(\lambda) = \frac{142}{(\lambda T)^5 \left[e^{14387/(\lambda T)} - 1 \right]}$$

where λ is in microns and T is in Kelvins. The star's output at 0.55μ is

$$S_0 = I/w(0.55) \text{ watts/cm}^2$$

Then,

$$S(\lambda) = S_0 w(\lambda) \text{ watts/cm}^2 - \mu$$

In photons/sec-cm² - μ , this is

$$\mathcal{Q}(\lambda) = 5 \times 10^{18} \lambda S(\lambda) \text{ photons/sec-cm}^2 - \mu$$

The last two columns of table 2 give the wavelength at which the maximum photon output occurs, $\lambda = 3669/T$, and the photon output at this wavelength.

While photon outputs are of interest for determining the suitability of specific stars for occultation sources, decisions about which wavelengths to use are based on atmospheric properties and the absorption characteristics of atmospheric constituents of interest. Applicable general and specific data are available in the literature^{7,8,9,10}. There are two obvious approaches to dealing with the abundance of stellar targets available at any time. The first is simply to examine the horizon at particular times and select whatever stars are within the field of view. The second is to preselect specific stars and observe them repeatedly as they rise and set on the horizon. This approach seems better suited to

long-term missions and, of course, it can be expanded to include as many stars as can be tracked during the course of the mission.

Fig. 5 gives some mission data for the 600-km, 57° orbit, when star number 13 (Sirius) is the target. Sirius has the highest photon output of any star considered at 1.0μ . Its declination is about -17° , so its terminator extends to latitudes of $\pm 73^\circ$. Application of the previous occultation geometry analysis shows that a 600-km, 57° orbit can view the southernmost ranges of the terminator, but not the northernmost, because the occultations can be viewed only from the "dark side" of the Earth. Also, for this orbit, there are several times during the year when the orbit plane's alignment relative to the stellar terminator is such that no star rises or sets are observable; this means that there is no time during the orbit when the spacecraft is 23.9° in central angle away from the terminator, along a great circle perpendicular to the terminator. Fig. 5(a) shows the tangent latitudes λ_T available with Sirius as a function of

time, but no constraints have been imposed. In particular, the location of the Sun has not been taken into account. Fig. 5(b) shows the angle η between unit vectors to the Sun and to Sirius--this angle is never less than about 40° for this particular star.

Fig. 5(c) shows solar elevation angle ζ_T over the tangent point;

these rather bizarre data can be thought of as resulting from the fact that the timing of the stellar occultations has no relationship to the motion of the Sun. Fig. 5(d) shows the pointing angle β for locating Sirius. (This angle is defined in fig. 6; it is the angle through which an instrument locked on the Earth's horizon would have to rotate to find the star.) The cyclic behavior of β makes possible the use of star rises as well as sets, due to the predictability of the star's future location on the horizon. Fig. 5(e) shows the apparent vertical velocity of the star at the horizon; this indicates the amount of time available for measurements. To the extent that v_{vert} remains constant

during a measurement, the time available to scan through H kilometers of atmosphere is $t = H/v_{\text{vert}}$. The cyclic patterns

in Fig. 5 will repeat themselves continuously. The initial position within the patterns is a function of launch timing, and is completely arbitrary from the present point of view--the launch date is mid-June, 1981, with the orbit plane orientation (time of day of launch) arranged such that it is approximately 6 a.m. local time, at the first equatorial crossing. In the parametric investigation of these orbits, it is necessary to keep in mind that only representative data can be produced until the time of launch (or insertion into orbit) is fixed. This time establishes the initial and subsequent relationship of the orbit plane to the celestial sphere, and hence, the time at which particular stellar targets become available. To summarize Fig. 5, each part

illustrates the type of cyclic variation which results for a particular quantity, with the entry point into the pattern dependent on the initial orbit plane orientation.

Fig. 7(a) is a repeat of 5(a), but includes the assumed constraint that occultations are useful only when the solar elevation angle at the tangent point is less than zero. Some other data of interest for viewing Sirius are shown in Fig. 7(b). The distribution of tangent latitudes and longitudes is of considerable interest for interpretation of the occultation measurements. For the 600-km, 57° orbit there are 5440 orbits in a year. During that time, there are 4900 star rises or sets for which the solar elevation angle is negative over the tangent point. Although it is not obvious from Fig. 7(b) how the longitude-latitude points are distributed in time, it can be shown that from rise to rise, or set to set, the tangent longitude changes by about 25° while the latitude changes a relatively very small amount.

With the results of viewing Sirius in mind, desired properties for additional targets become apparent. One or more stars are needed with a small positive declination, to give high northern latitude coverage, and stars need to be found which will have right ascensions and declinations such that coverage will be available during a time when no occultations of Sirius are possible. Fig. 8 shows the RA- δ distribution of the 25 brightest IR stars. It can be seen from Figs. 5 and 7 that continuous coverage in the higher northern and southern latitudes cannot be obtained with a single star, so the near-equatorial stars in Fig. 8 could be used to provide additional sources for such coverage on a frequent basis. Of the stars shown in Fig. 8, 10 are within $\pm 20^\circ$ of the equator. Tangent latitude coverage for all 10 of these stars, including Sirius, are given in Fig. 9.

Figs. 10 and 11 show, respectively, tangent latitude coverage for the Sun-synchronous and 250-km, 28° orbits, using the same 10 stars as in Fig. 9. The Sun-synchronous data are characterized by large gaps in the coverage available with each star because of unfavorable lighting conditions at the tangent point, as well as long periods of time when occultations are geometrically not possible. Such periods tend to last longer than for the lower inclination orbits because of the relatively slow precession of the orbital plane. It is worth emphasizing at this point that the lighting-related gaps are produced not by the spacecraft orbit, nor by the time of launch, but just by the relationship of the Sun to the star on the celestial sphere.

For the 250-km, 28° orbit, occultations are always possible with the 10 low-declination stars, so the only gaps in coverage are due to lighting conditions at the tangent point. Recalling table 1,

latitude coverage is available only for $\pm 44^\circ$, making this orbit least suitable, of the three discussed in this paper, for "global" measurements. It is, nonetheless, representative of the type of Space Shuttle orbits available in the near future, and deserves study just for that reason.

COMPARISON WITH SOLAR OCCULTATION MISSIONS

As noted previously, single-star occultation missions produce latitude coverage patterns very similar to those observed for solar occultation. In Fig. 12(a), the tangent latitude of solar occultations is plotted as a function of time for the 600-km, 57° orbit. Tangent latitudes are available from $\pm 80.9^\circ$, depending on the Sun's declination--equivalent to time of year of the launch. The seasonal motion of the Sun is clearly seen in the figure. Gaps in the coverage occur whenever the solar terminator is positioned so that the orbit plane is never 23.9° away in central angle, as discussed previously for certain stellar declinations. For the 28° orbit, this seasonal motion would not be so apparent, and the data would be virtually indistinguishable from that obtained with a star like Sirius. The main difference would be in the cycle time for the coverage patterns; for stellar occultations, the orbit plane precession rate relative to inertial space is what determines the cycle time, while for solar occultations, the precession relative to the Sun is what matters. For Sun-synchronous orbits, the initial spacecraft-Sun geometry is maintained, on the average, by definition. Hence the data are not easily compared with stellar occultations done from Sun-synchronous orbits, where precession of the orbit plane in inertial space at about $1^\circ/\text{day}$ (the average rate of the Sun) causes the geometry constantly to change. Fig. 12(b) gives, for comparison with 5(d), the pointing angle β required to follow Sun rises and sets from a 600-km, 57° orbit during a 1-year mission.

DISCUSSION OF RESULTS

Generally, it is believed that surveys of atmospheric parameters need to be done on a large geographical scale in as short a time as possible. Specifically, surveys through a large range of latitudes will prove valuable for global modeling. This is because longitudinal variations tend to be less pronounced than latitudinal variation, due to the east-west patterns of atmospheric circulation. Short-term solar occultation missions are being proposed^{11,12} in which one of the primary design objectives is to maximize latitudinal coverage by proper choice of launch timing. With stellar occultation, such sweeps through a range of tangent latitudes are available with much higher frequency, by picking low-declination stars and following each of them in succession for several days as orbit precession drives the tangent points through the available

range of values. With solar or stellar occultation, there is an accumulation of many measurements at the extremes of latitude due to the way in which orbit precession causes the geometry to change. With stellar occultation, these data can be taken only if needed--if not, another star can be selected.

The tangent latitude coverage shown in Figs. 9, 10, and 11 is difficult to follow in detail even with partial identification of the data, as given. However, complete identifications are easily made whenever required. Each star viewed from a given orbit has associated with it a particular tangent latitude vs. time signature and a fixed set of pointing angle requirements. These characteristics are determined by the star's right ascension and declination. The sequencing of possible measurements is determined by the relative positions of stars and the Sun on the celestial sphere. With the 600-km, 57° orbit, nearly all the Earth's surface can be covered repeatedly with proper choice of targets.

With the procedures established for analysis of this type of mission, detailed investigations of stellar occultation opportunities during long-term missions can become narrowly focused when basic orbit parameters are actually known. Orbit altitude and inclination are the principal factors in determining star availability. Once these are specified, tangent latitude vs. time data can be generated for as many stars as desired, similar to Fig. 5(a). These data, unconstrained by other factors, are actually functions of orbit plane orientation rather than time, per se. Hence, the characteristic pattern for each star can be obtained by just rotating the orbit plane through 360°. The same argument applies to pointing angle and v_{vert} , as in Figs. 5(d) and (e). But, additional orbit constraints are needed. Sun-lighting conditions at the tangent point are seasonally variable due to the Sun's motion. Thus, each star's characteristic occultation patterns must be modified--removing some of the geometrically available measurements--according to time of year. It is also possible to envision cases where Sun elevation angle is negative at the tangent point, but the central angle between Sun and star, η , is still small enough to cause signal-to-noise problems. This would correspond to a dawn or dusk situation on the ground under the measurement. These limits have to be established; their impact would be to remove a few more occultation opportunities from consideration. It is possible, too, that daylight conditions could be allowed during the measurement if the central angle between Sun and star is large enough. Within whatever limits are finally established, it can be shown that the measurement opportunities will be uniformly distributed with respect to solar elevation angle. This is reasonable just because of the lack of coordination between the timing of measurements and the position of the Sun. Looked at another way, this circumstance provides a uniform distribution of local times

for the measurements, within the allowed range of times. This is in sharp contrast to solar occultation, where measurements are always made, by definition, at local sunrise or sunset.

SUMMARY

A geometrical analysis of stellar occultations viewed from orbit has been considered for 1-year missions with three different orbits: 600-km, 57° ; 250-km, 28° , and 888-km, Sun-synchronous. Simulated mission data presented include representative samples of geographical coverage, pointing angle, vertical tracking rate requirements, and information on solar position. The scenario involves following a relatively small number of preselected stars throughout the course of the mission. For this paper, 10 stars have been chosen on the basis of their low declination and brightness at a wavelength of 1.0μ . This is an arbitrary choice, and relevant data for 158 bright stars have been provided to facilitate other choices in the future. Low declination stars insure that the stellar "terminator" reaches high northern and southern latitudes so that coverage of large portions of the globe can be obtained. Such coverage is easily available for longitude, but latitude coverage must be planned carefully in advance to benefit from the geometrical properties of stellar occultation measurements made from orbit; these include periods of time when no occultations are possible, Sun lighting restrictions, and opportunities for spanning the entire available latitude range in a relatively short period of time. Maximum utilization of the last of these characteristics would form the basis for detailed mission planning in the future. A brief comparison with solar occultation measurements made from the 600-km, 57° orbit demonstrates the geometrical limitations of a single-source technique compared to the potential available with stellar occultations.

REFERENCES

1. Brooks, David R.: An Introduction to Orbit Dynamics and Its Application to Satellite-Based Earth Monitoring Missions. NASA-RP 1009, Washington, DC, Nov. 1977.
2. Russell, Phillip B., Ed.: SAGE Ground Truth Plan--Correlative Measurements for the Stratospheric Aerosol and Gas Experiment (SAGE) on the AEM-B Spacecraft. NASA TM-80076, March 1979.
3. Atreya, S. K.; Donahue, T. M.; Sharp, W. E.; and Wasser, B.: Ultraviolet Stellar Occultation Measurement of the H_2 and O_2 Densities Near 100 km in the Earth's Atmosphere. Geophysical Research Letters, vol. 3, no. 10, Oct. 1976.

4. Hays, P. B.; and Roble, R. G.: Observation of Mesospheric Ozone at Low Latitudes. Planetary and Space Sciences, vol. 21, Feb. 1973, pp. 272-279.
5. Hays, P. B.; and Roble, R. G.: Stellar Occultation Measurements of Molecular Oxygen in the Lower Thermosphere. Planetary and Space Sciences, vol. 21, Mar. 1973, pp. 339-348.
6. Williams, Charles S.; and Becklund, Orville A.: Optics: A Short Course for Engineers and Scientists. Wiley-Interscience, NY, NY, 1972.
7. Valley, Shea L., Scientific Editor: Handbook of Geophysics and Space Environments. Air Force Cambridge Research Laboratories, 1965.
8. Watanabe, K.; Zelikoff, Murray; Inn, Edward C. Y.: Absorption Coefficients of Several Atmospheric Gases. Air Force Cambridge Research Center, AFCRC Technical Report No. 53-23, Geophysical Research Papers, No. 21, June 1953.
9. Park, Jae H.: Atlas of Infrared Absorption Lines. NASA Contractor Report CR-2925, Contract NSG-1203, November 1977.
10. Sullivan, J. O.; and Holland, A. C.: A Congeries of Absorption Cross Sections for Wavelengths Less Than 3000 Å. NASA Contractor Report CR-371, Contract NASw-840, January 1966.
11. Brooks, David R.; and Harrison, Edwin F.: Orbit Design for Solar and Dual Satellite Occultation Measurements of Atmospheric Constituents. 1977 AAS/AIAA Astrodynamics Conference, Jackson Lake Lodge, Wyoming, September 7-9, 1977.
12. Harrison, Edwin F.; Lawrence, George F.; and Lamkin, Stanley L.: Mission Analysis for Atmospheric Measurements Using Solar Occultation Experiments on Shuttle Spacelabs. Paper 79-102, AAS/AIAA Astrodynamics Specialist Conference, Provincetown, Mass., June 25-27, 1979.

Table 1
 ORBIT PARAMETERS FOR THREE REPRESENTATIVE EARTH ORBITS USED
 IN A PARAMETRIC SURVEY OF STELLAR OCCULTATION OPPORTUNITIES

i , deg	h , km	τ , sec [†]	$\dot{\Omega}$, deg/day	A , deg [‡]	tangent latitude range, deg
28	250	5353	-7.6972	15.8	+44
57	600	5800	-3.9614	23.9	+81
98.988*	888	6171	0.9856	28.6	+90

* Sun-synchronous orbit with a repeat cycle of 1 day
 (Q=14).

† τ is nodal period.

‡ Central angle separation between spacecraft and terminator, measured along a great circle perpendicular to the terminator, at which occultations are possible.

Table 2
DATA FOR 158 BRIGHT STARS

n	RA _s , deg	δ _s , deg	m _v	T, Kelvins	n	RA _s , deg	δ _s , deg	m _v	T, Kelvins
1	1.721	28.930	2.1	9450	54	106.803	-26.346	2.0	6200
2	10.533	-18.146	2.2	5170	55	113.188	31.953	1.6	9450
3	13.736	60.560	2.1	28000	56	125.480	-59.416	1.7	5170
4	24.159	-57.384	0.6	16500	57	130.976	-54.602	2.0	9450
5	31.030	89.131	2.1	6200	58	187.387	-56.951	1.6	3480
6	44.290	-40.420	3.4	8900	59	191.503	-59.531	1.5	22500
7	45.190	3.977	2.8	3520	60	193.190	56.117	1.7	9450
8	50.561	49.759	1.9	6500	61	262.909	-37.084	1.7	20300
9	68.564	16.452	1.1	4350	62	263.808	-42.981	2.0	7200
10	78.286	-8.234	0.3	13000	63	275.562	-34.400	1.9	9450
11	78.636	45.970	0.2	5970	64	1.905	58.990	2.4	6500
12	95.827	-52.679	-0.9	7200	65	6.213	-42.464	2.4	5170
13	100.968	-16.675	-1.6	9450	66	17.025	35.467	2.4	3520
14	114.446	5.300	0.5	6500	67	30.527	42.191	2.3	5170
15	122.160	-47.251	1.9	30000	68	82.631	0.000	2.5	28000
16	134.308	48.157	3.1	8220	69	86.595	-9.679	2.2	28000
17	141.540	-8.532	2.2	4830	70	89.350	44.946	2.1	9450
18	151.707	12.109	1.3	13000	71	110.737	-29.246	2.4	16500
19	176.895	14.734	2.2	8900	72	120.641	-39.921	2.3	30000
20	183.578	-17.381	2.8	13000	73	136.732	-43.315	2.2	4350
21	186.243	-62.939	1.0	22500	74	139.079	-59.153	2.2	7200
22	200.915	-11.011	1.2	20300	75	165.025	56.538	2.4	9450
23	206.600	49.458	1.9	18800	76	200.690	55.076	2.4	8900
24	211.242	-36.228	2.3	5170	77	222.693	74.274	2.2	4350
25	213.584	19.332	0.2	5170	78	268.983	51.492	2.4	4350
26	233.365	26.811	2.3	9450	79	305.297	40.163	2.3	6200
27	246.906	-26.369	1.2	3520	80	331.603	-47.102	2.2	16500
28	251.395	-68.977	1.9	4830	81	340.235	-47.037	2.2	3480
29	263.397	12.580	2.1	8220	82	9.712	56.379	2.3	5170
30	278.989	38.756	0.1	9450	83	178.078	53.856	2.5	9450
31	283.367	-26.334	2.1	18800	84	239.654	-22.541	2.5	28000
32	297.342	8.791	0.9	8220	85	252.070	-34.242	2.4	5170
33	304.845	-14.874	3.2	5970	86	2.935	15.022	2.9	20300
34	305.840	-56.830	2.1	18800	87	265.120	-39.017	2.5	20300
35	310.110	45.176	1.3	8900	88	20.976	60.085	2.8	8220
36	325.690	9.741	2.5	5170	89	28.008	20.667	2.7	8220
37	344.012	-29.776	1.3	8630	90	56.439	24.017	3.0	16500
38	31.383	23.326	2.2	4830	91	58.076	31.799	2.9	22500
39	47.710	-29.101	3.9	6200	92	58.975	39.928	3.0	22500
40	115.886	28.097	1.2	5170	93	73.775	33.122	2.9	4830
41	138.223	-69.598	1.8	9450	94	76.606	-5.123	2.9	8680
42	165.488	61.908	1.9	5170	95	81.750	-20.782	3.0	5970
43	189.977	-48.801	2.4	9450	96	82.863	-17.842	2.7	7200
44	219.404	-60.717	0.1	5970	97	83.503	-5.928	2.9	30000
45	88.400	7.403	1.0	3520	98	83.977	21.126	3.0	18800
46	210.440	-60.234	0.9	22500	99	84.650	-34.089	2.7	16500
47	80.894	6.325	1.7	20300	100	89.436	37.212	2.7	9450
48	81.114	28.584	1.8	13000	101	102.304	-50.579	2.8	5170
49	83.685	-1.219	1.7	28000	102	109.030	-37.044	2.7	4350
50	84.824	-1.957	2.0	28000	103	121.577	-24.220	2.9	6500
51	95.355	-17.941	2.0	22500	104	140.304	-54.886	2.6	18800
52	99.009	16.425	1.9	9450	105	154.594	19.989	2.6	5170
53	104.371	-28.932	1.6	22500	106	161.379	-49.267	2.8	5570

Table 2 (concluded)

n	RA _s , deg	δ _s , deg	m _v	T, Kelvins
107	168.142	20.683	2.6	8680
108	188.215	-23.237	2.8	5570
109	188.859	-68.976	2.9	18800
110	190.047	-1.291	2.9	7200
111	193.668	38.474	2.9	9450
112	195.183	11.115	2.9	5170
113	199.740	-36.560	2.9	8900
114	204.510	-53.320	2.6	22500
115	208.326	18.542	2.8	5970
116	217.727	38.434	3.0	7200
117	218.414	-42.031	2.6	18800
118	219.998	-47.265	2.9	20300
119	220.930	27.196	2.7	5170
120	222.317	-15.922	2.9	8680
121	239.156	-43.018	2.8	20300
122	228.861	-9.277	2.7	13000
123	233.300	-41.071	2.9	18800
124	235.709	6.516	2.7	5170
125	239.273	-26.032	3.0	20300
126	240.937	-19.727	2.9	22500
127	245.898	61.579	2.9	5570
128	247.243	21.552	2.8	5170
129	248.518	-28.158	2.9	28000
130	248.890	-10.510	2.7	28000
131	250.048	31.654	3.0	5970
132	257.178	-15.691	2.6	8900
133	260.721	-55.505	2.8	4830
134	262.197	-37.274	2.8	18800
135	262.399	-49.855	3.0	18800
136	262.444	52.322	3.0	5970
137	265.510	4.578	2.9	5170
138	274.784	-29.842	2.8	5170
139	276.545	-25.439	2.9	5170
140	285.192	-29.923	2.7	8900
141	296.017	45.059	3.0	9450
142	296.220	10.541	2.8	4830
143	311.259	33.861	2.6	5170
144	319.472	62.462	2.6	8220
145	326.360	-16.260	3.0	8220
146	334.132	-60.405	2.9	4830
147	345.591	27.925	2.6	3520
148	345.828	15.049	2.6	9450
149	29.464	-61.711	3.0	7200
150	34.470	-3.109	3.0	3050
151	46.569	40.845	3.0	13000
152	142.585	-56.906	3.0	4350
153	160.480	-64.242	3.0	28000
154	181.712	-50.561	2.9	18800
155	238.142	-63.343	3.0	7200
156	286.019	13.819	3.0	9450
157	287.010	-21.071	3.0	6850
158	243.206	3.621	3.0	3520

Table 3
PHOTON OUTPUTS FOR 10 BRIGHT STARS

n	m _v	T, Kelvins	Photons/sec-cm ² -μ at λ =				λ _{max}	Output
			0.1	0.55	1.0	10		
7	2.8	3520	1.8x10 ⁻⁶	6.5x10 ⁵	1.7x10 ⁶	2.0x10 ⁴	1.042	1.7x10 ⁶
9	1.1	4350	5.0x10 ⁻³	3.1x10 ⁶	4.4x10 ⁶	2.9x10 ³	0.843	4.6x10 ⁶
10	0.3	13000	6.0x10 ⁵	6.5x10 ⁶	1.9x10 ⁷	3.3x10 ³	0.282	1.2x10 ⁷
13	-1.6	9450	1.2x10 ⁵	3.7x10 ⁶	1.4x10 ⁷	3.1x10 ⁴	0.388	4.5x10 ⁷
14	0.5	6500	6.6x10 ¹	5.4x10 ⁶	3.3x10 ⁶	1.1x10 ⁴	0.564	5.4x10 ⁶
25	0.2	5170	8.3x10 ⁻¹	7.1x10 ⁶	6.7x10 ⁶	3.2x10 ³	0.709	8.1x10 ⁶
32	0.9	8220	2.0x10 ³	3.7x10 ⁶	1.6x10 ⁶	4.1x10 ³	0.446	4.0x10 ⁶
45	1.0	3520	9.3x10 ⁻⁶	3.4x10 ⁵	8.9x10 ⁶	1.0x10 ⁵	1.042	9.0x10 ⁶
150	3.0	3050	8.5x10 ⁻⁹	5.4x10 ⁵	2.4x10 ⁶	4.3x10 ⁴	1.202	2.5x10 ⁶
158	3.0	3520	1.5x10 ⁻⁶	5.4x10 ⁵	1.4x10 ⁶	1.6x10 ⁴	1.042	1.4x10 ⁶

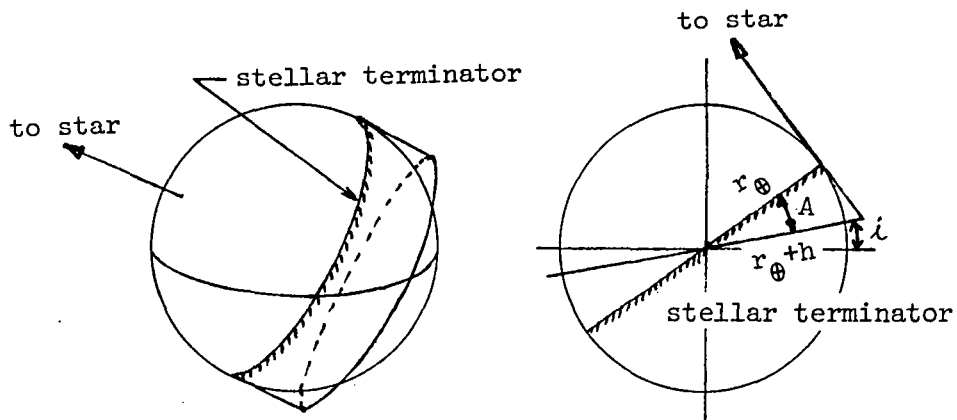


Fig. 1 Geometry for stellar occultation measurements

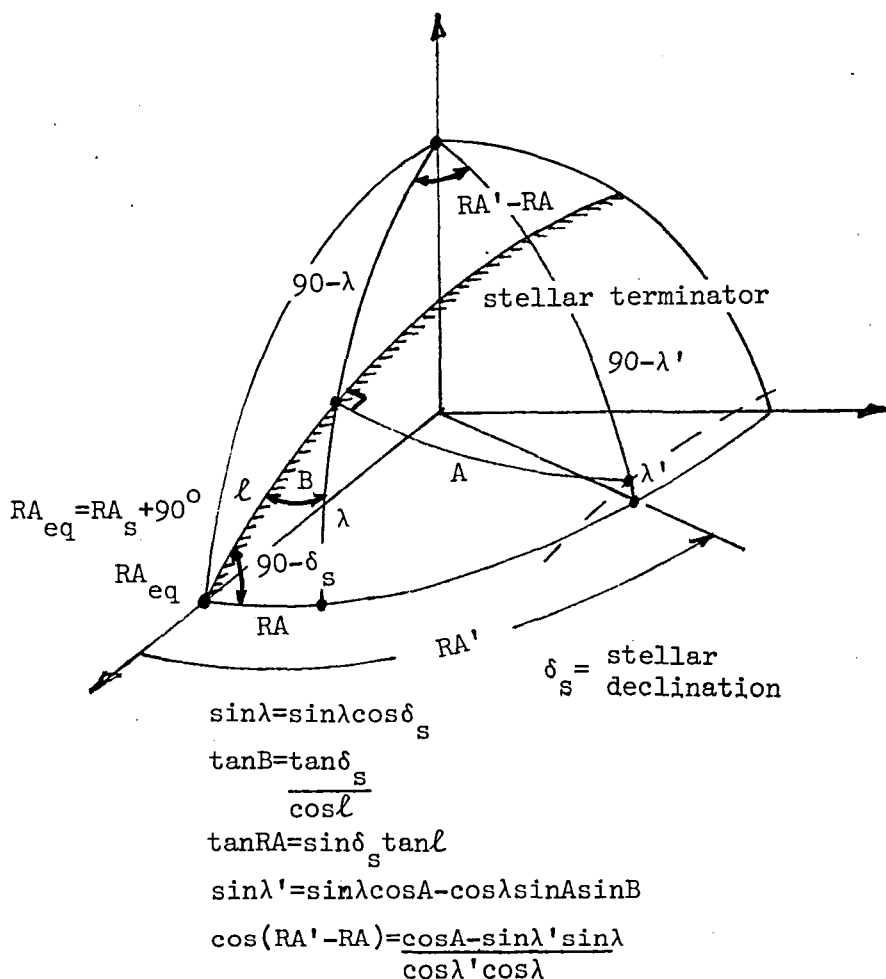


Fig. 2 Calculation of ground coordinates above which stellar occultation measurements may be made

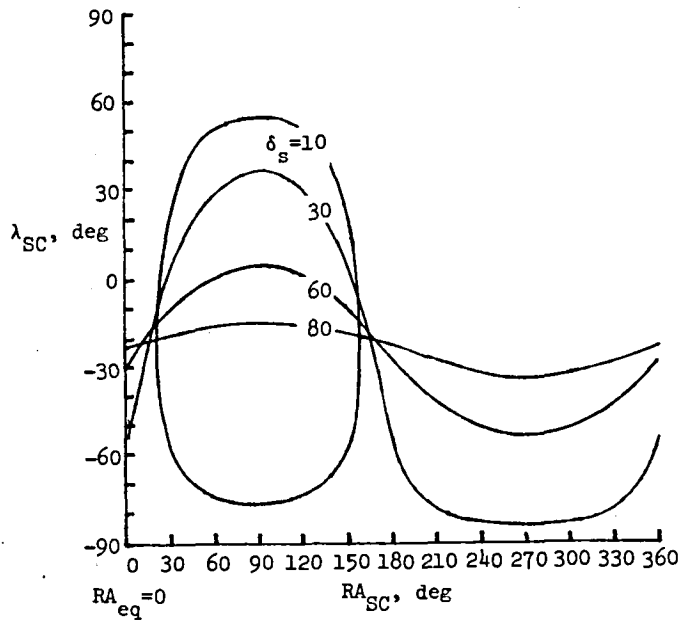


Fig. 3 Spacecraft coordinates from which stellar occultations can be viewed as a function of stellar declination δ_s from a 600-km orbit

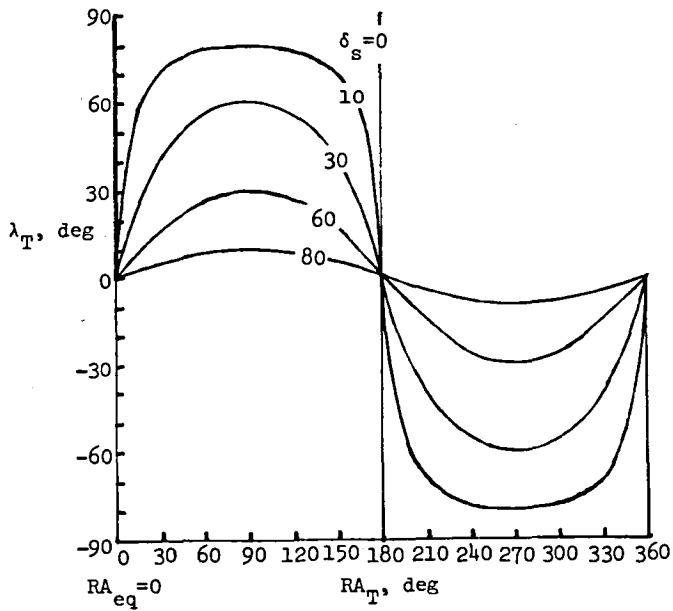
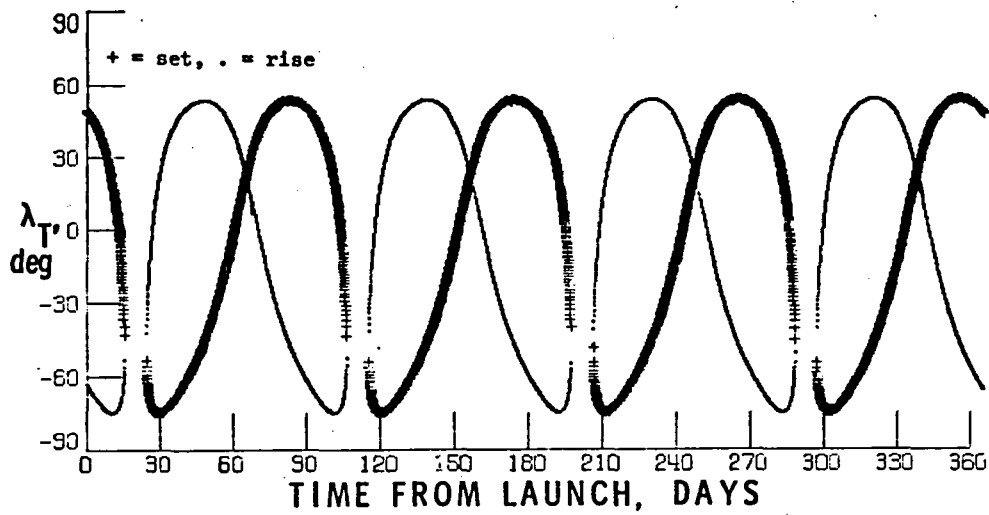
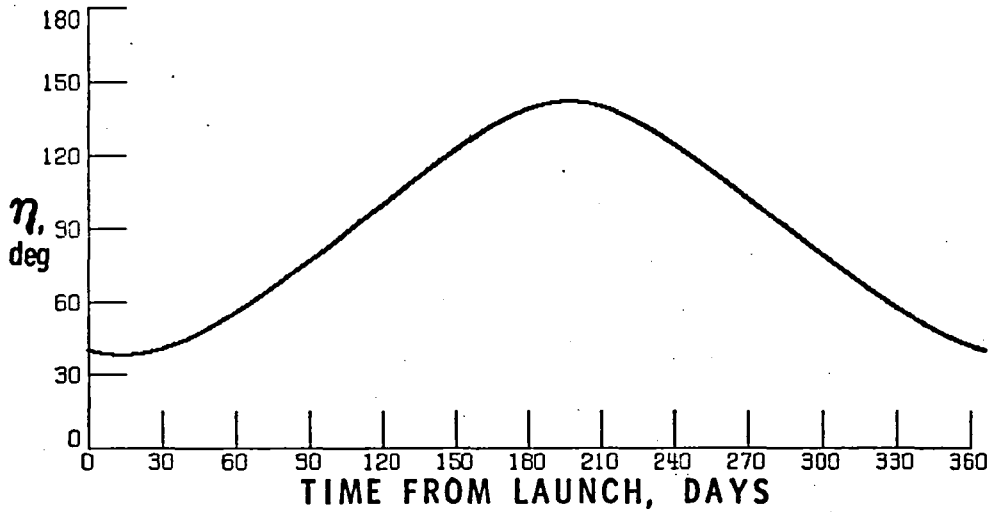


Fig. 4 Tangent coordinates at which stellar occultation measurements will be made as a function of stellar declination δ_s

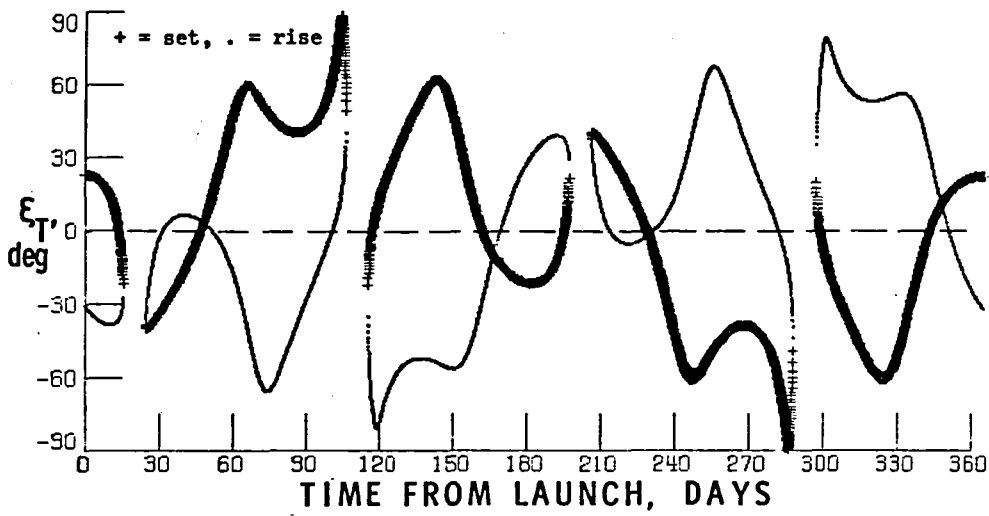


(a) tangent latitude as a function of time

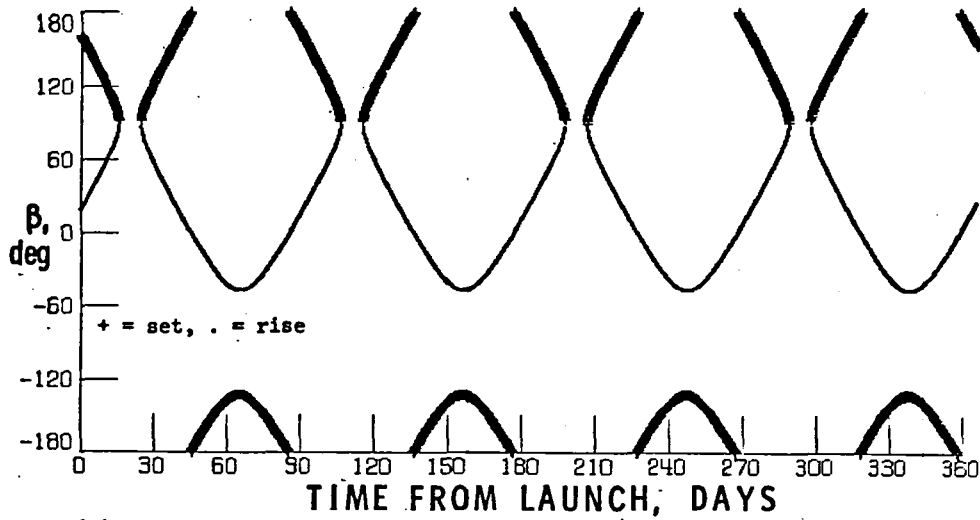


(b) angle between unit vectors to Sirius and the Sun as a function of time

Fig. 5 Unconstrained occultation data for Sirius, viewed from a 600-km, 57° orbit

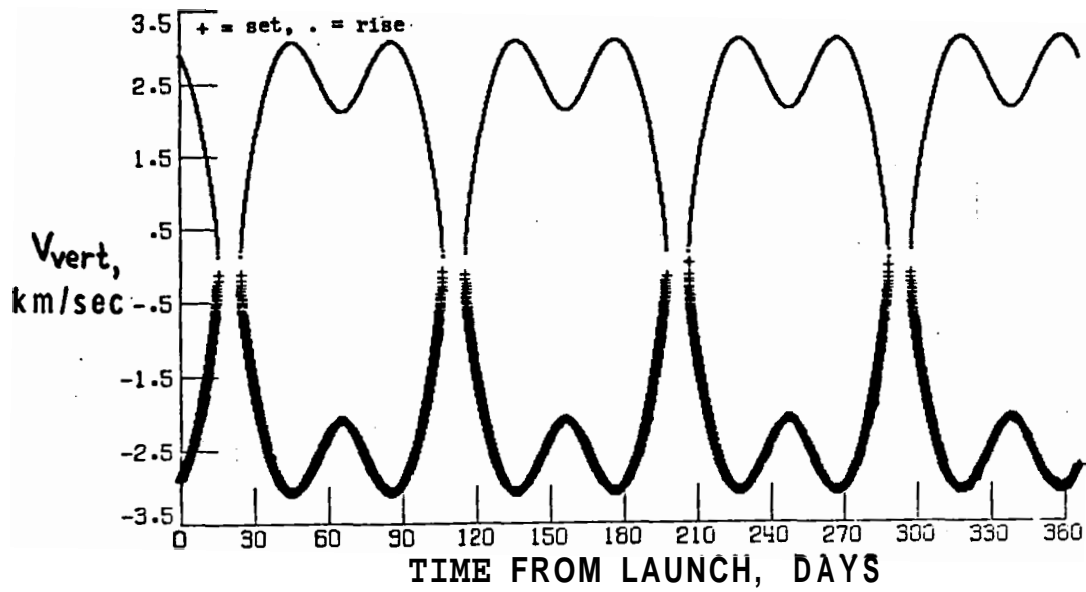


(c) solar elevation angle ϵ_T' at the tangent point as a function of time



(d) pointing angle β as a function of time

Fig. 5 (continued)



(e) v_{vert} as a function of time

Fig. 5 (concluded)

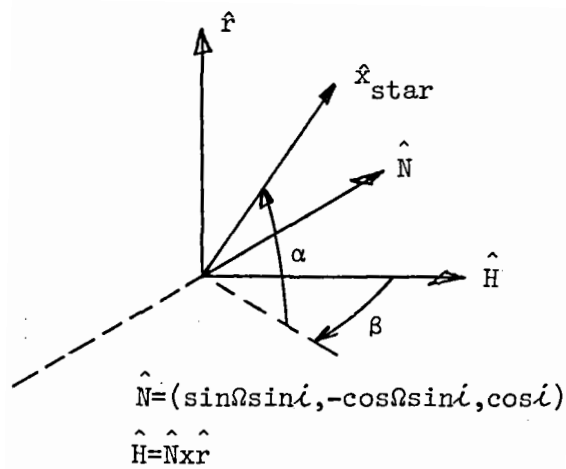
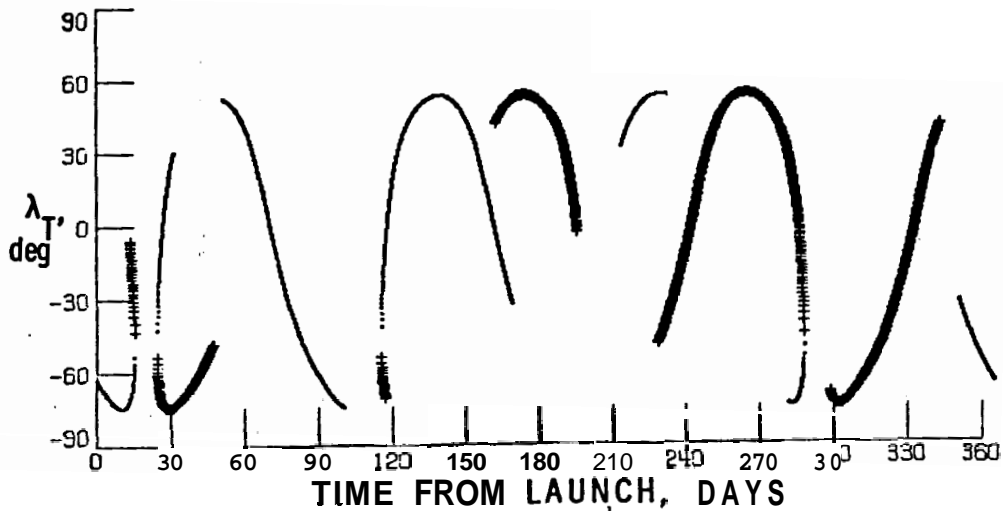
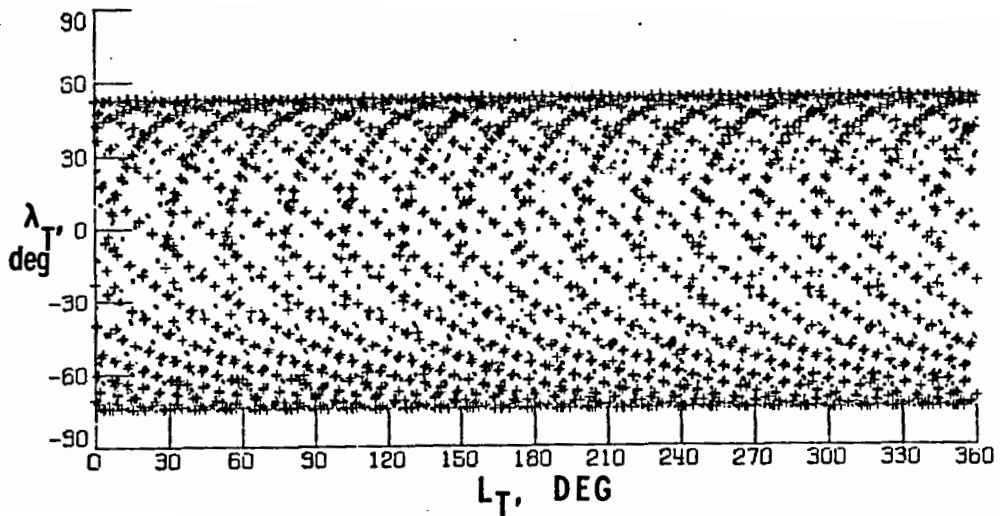


Fig. 6 Definition of the pointing angle β as a function of time



(a) tangent latitude as a function of time



(b) tangent latitude vs. tangent longitude

Fig. 7 Occultation data for Sirius, viewed from a 600-km, 57° orbit, with the constraint that solar elevation angle must be less than zero at the tangent point

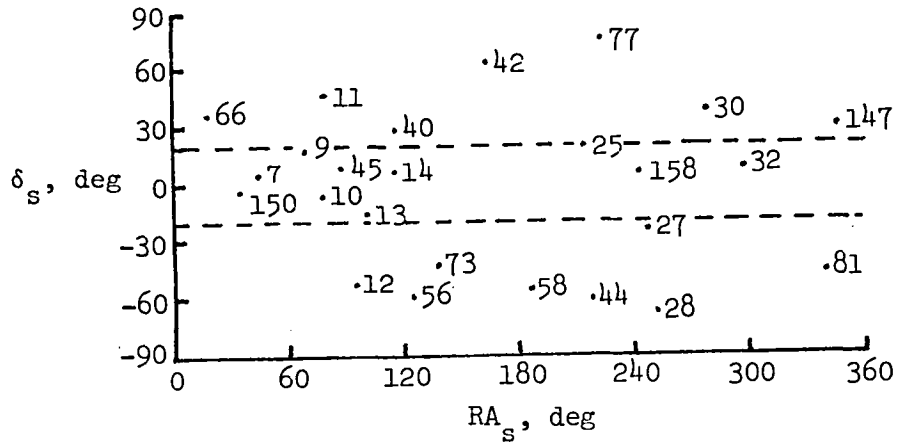


Fig. 8 Right ascension and declination of the 25 brightest IR stars

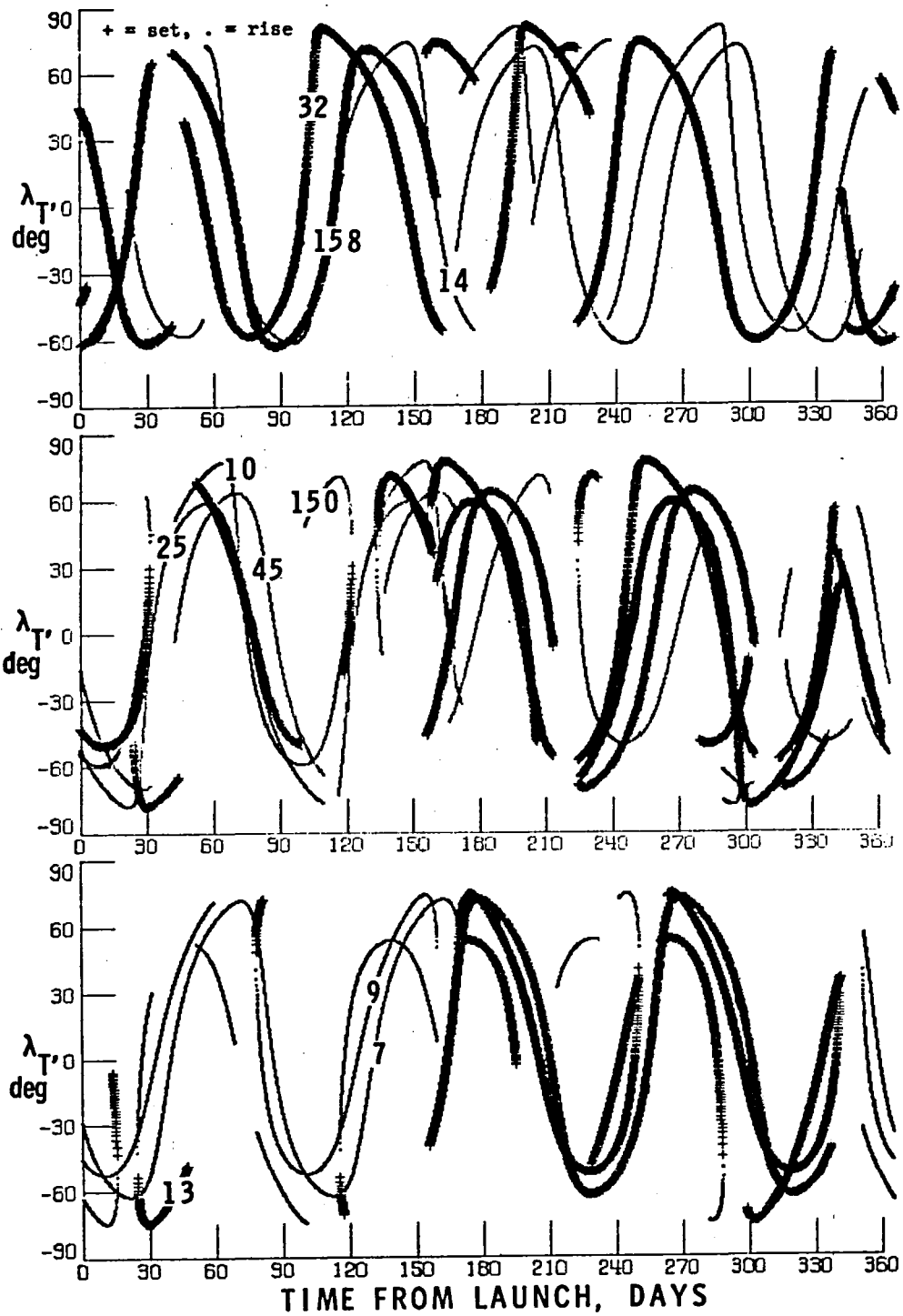


Fig. 9 Tangent latitude as a function of time for 10 bright IR stars viewed from a 600-km, 57° orbit

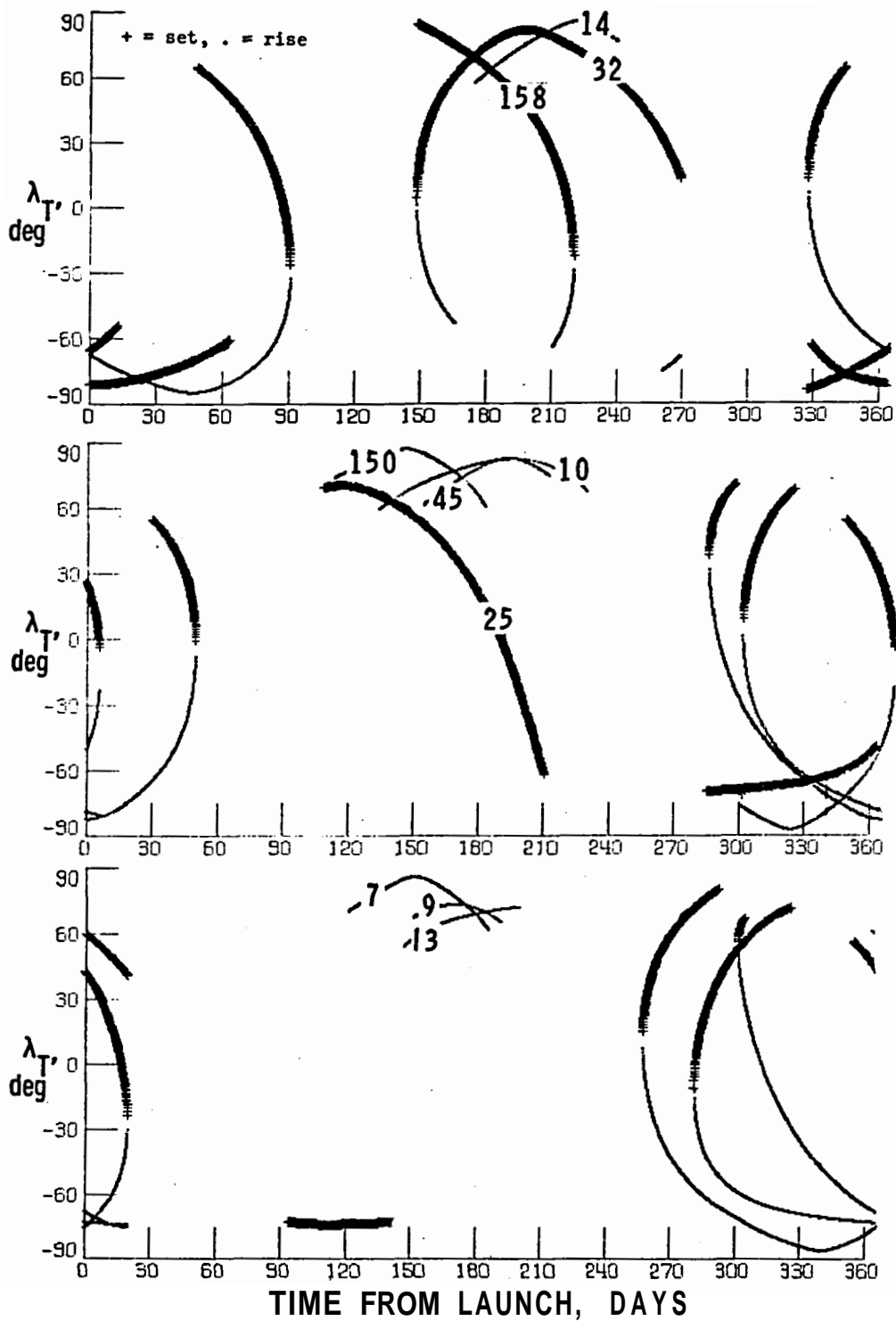


Fig. 10 Tangent latitude as a function of time for 10 bright IR stars viewed from a 888-km Sun-synchronous orbit

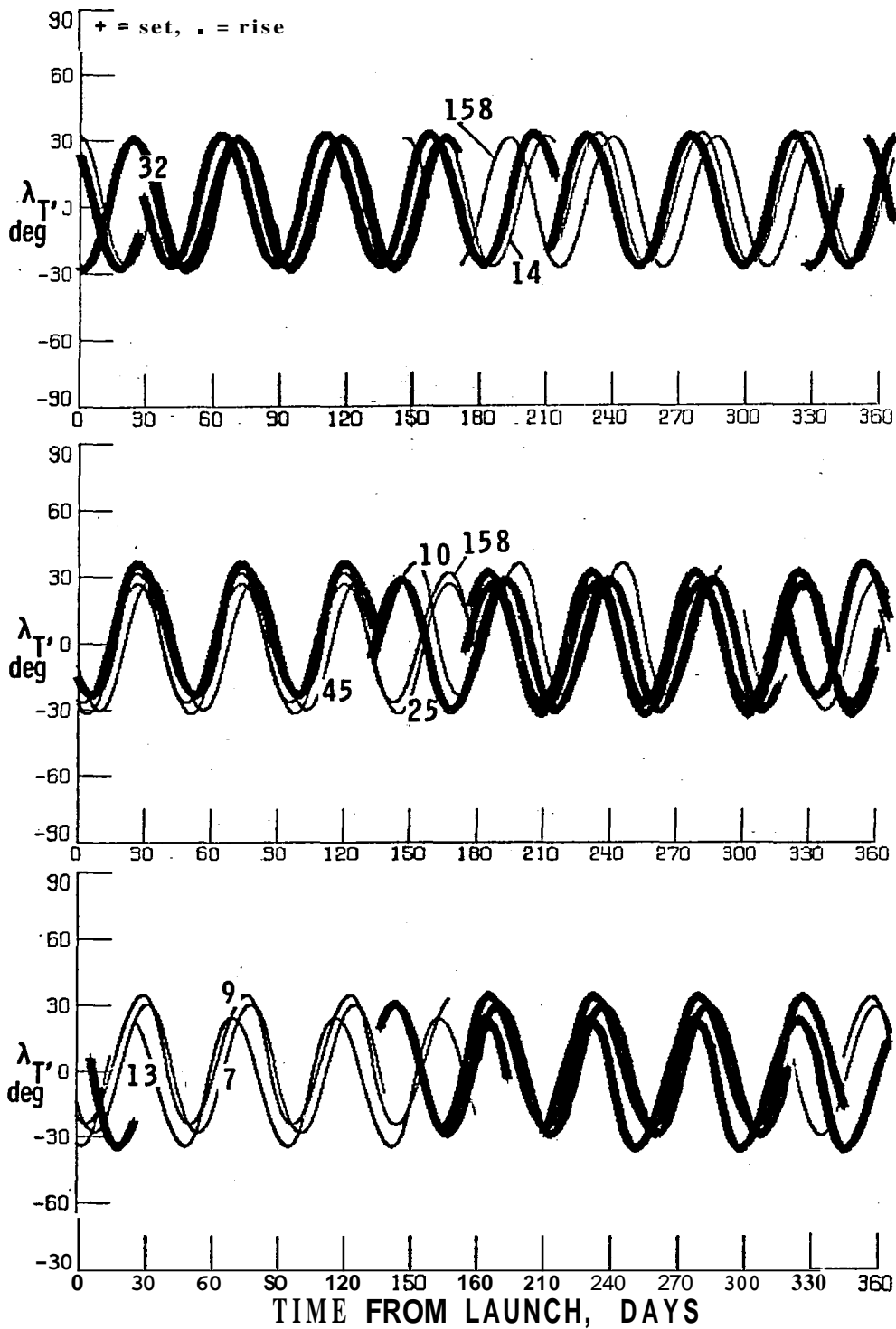
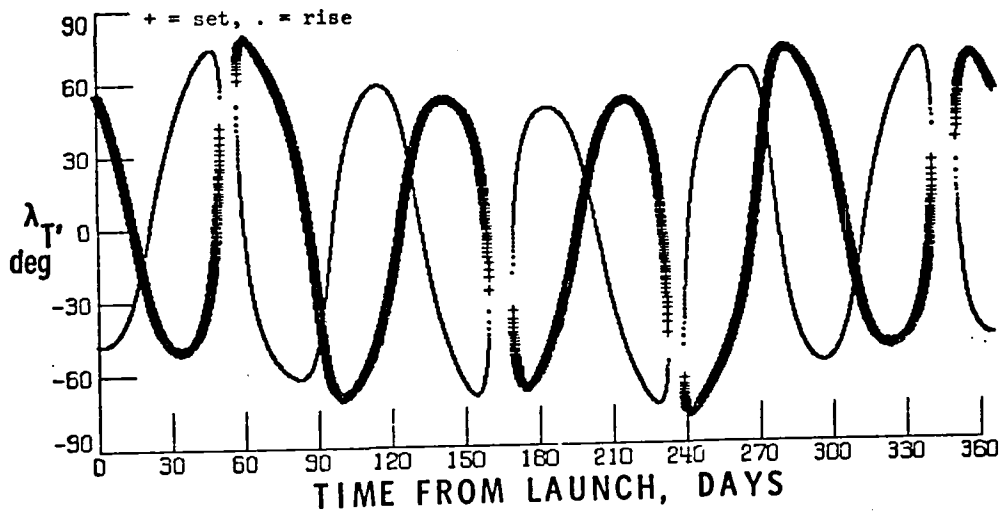
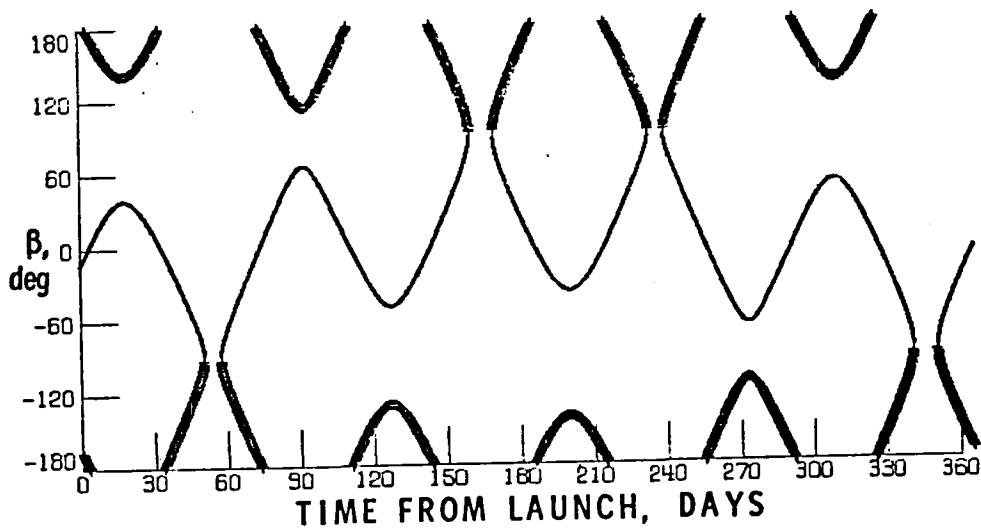


Fig. 11 Tangent latitude as a function of time for 10 bright IR stars viewed from a 250-km, 28° orbit



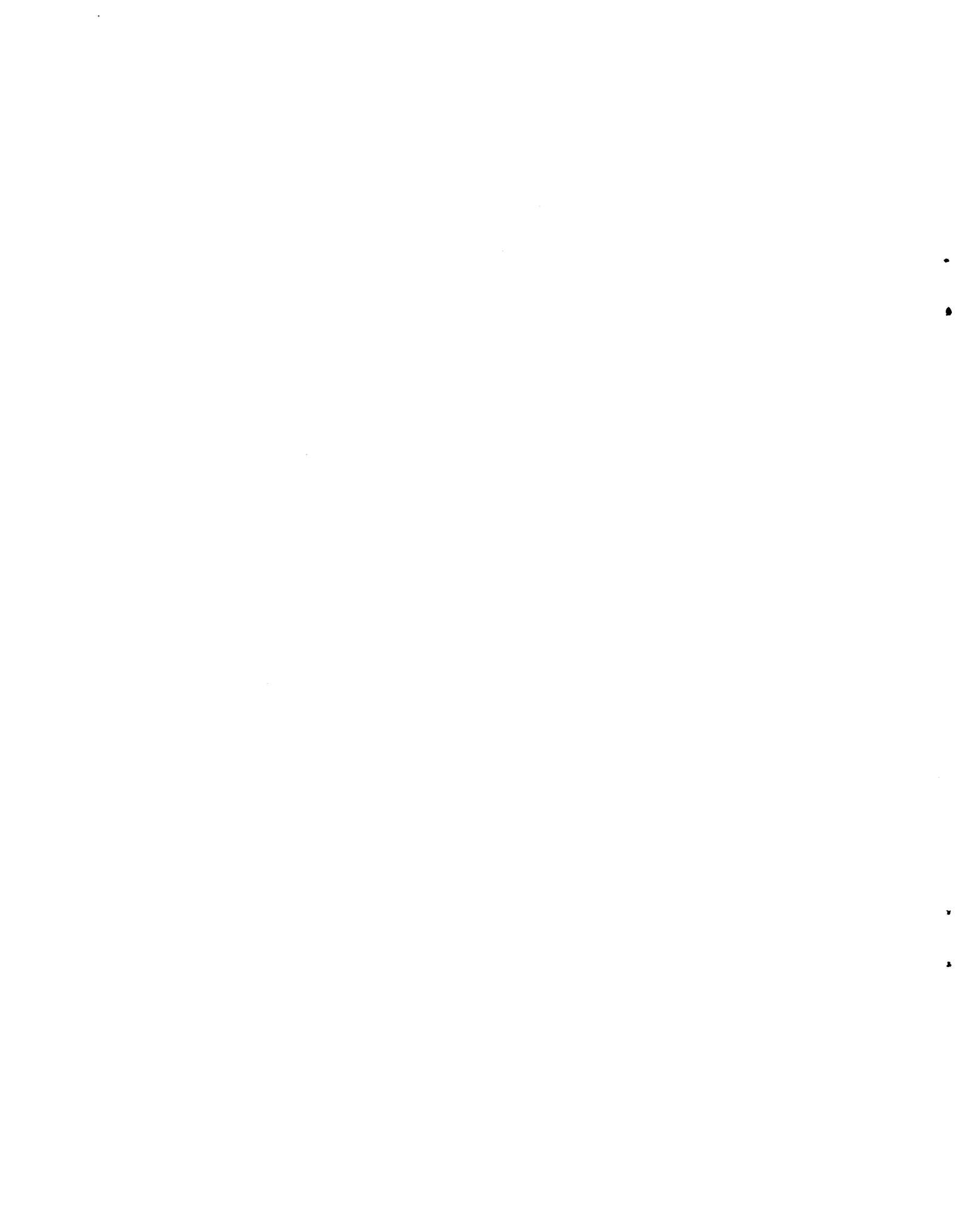
$t = 0$ in mid-June, 1981

(a) tangent latitude as a function of time



(b) pointing angle β as a function of time

Fig. 12 Solar occultation data obtained from a 600-km, 57° orbit



1. Report No. NASA TM-80138		2. Government Accession No.		3. Recipient's Catalog No.	
4. Title and Subtitle The Geometry of Stellar Occultation Measurements On Long-Duration Atmospheric Monitoring Missions				5. Report Date July 1979	
				6. Performing Organization Code	
7. Author(s) David R. Brooks				8. Performing Organization Report No.	
9. Performing Organization Name and Address National Aeronautics and Space Administration Langley Research Center Hampton, Virginia 23665				10. Work Unit No. 146-20-14-01	
				11. Contract or Grant No.	
12. Sponsoring Agency Name and Address National Aeronautics and Space Administration Washington, D.C. 20546				13. Type of Report and Period Covered Technical Memorandum	
				14. Sponsoring Agency Code	
15. Supplementary Notes Paper 79-101 presented at the AAS/AIAA Astrodynamics Specialist Conference, Provincetown, Mass., June 25-27, 1979.					
16. Abstract <p>Geometrical considerations are presented for analyzing use of the stellar occultation technique on long-duration Earth atmosphere monitoring missions. Simulated mission data are presented for three representative orbits. Bright near-IR stars are used as examples of how extensive global longitude-latitude coverage can be obtained by performing occultation measurements on several stars during the course of a 1-year mission. A brief comparison is made with similar missions using the Sun as a light source.</p>					
17. Key Words (Suggested by Author(s)) Earth orbit dynamics, mission analysis, atmospheric monitoring			18. Distribution Statement Unclassified - Unlimited Subject Category 13		
19. Security Classif. (of this report) UNCLASSIFIED		20. Security Classif. (of this page) UNCLASSIFIED		21. No. of Pages 25	22. Price* \$4.00

